BRANZ

STUDY REPORT

No. 175 (2007)

Creep and Shrinkage of Inorganic Polymer Concrete

NP Lee

The work reported herein was funded by the Building Research Levy and supported by Golden Bay Cement.

ISSN: 0113-3675

Preface

This is a brief report examining the creep and early age shrinkage behaviour of inorganic polymer concretes (IPCs). These innovative new construction materials utilise a binder produced by the reaction of a strongly alkaline sodium silicate solution with fly-ash from the combustion of coal. Field experience suggests that IPC can be laid in much longer continuous runs than an equivalent Portland cement concrete without the risk of drying shrinkage cracking. The testing discussed here is an attempt to determine whether this behaviour can be attributed to stress relaxation via a creep mechanism.

Acknowledgments

Golden Bay Cement generously allowed access to their proprietary mix designs and contributed the raw materials production of the IPCs examined in this report. The cooperation and expertise of Technical Manager, Warren South, and especially the time and effort spared by Technician Jason Goile are gratefully acknowledged.

This work was funded by the Building Research Levy.

Note

This report is intended for concrete engineers, materials scientists and other industry practitioners with an interest in the practical application of inorganic polymer (*aka* geopolymer) concrete.

Creep and Shrinkage of Inorganic Polymer Concrete

BRANZ Study Report SR 175

NP Lee

Reference

Lee NP. 2007. 'Creep and Shrinkage of Inorganic Polymer Concrete'. BRANZ *Study Report SR 175*. BRANZ Ltd, Judgeford, New Zealand.

Abstract

The creep and free shrinkage of a series of fly-ash derived inorganic polymer concretes (IPCs) were measured in an attempt to explain observed in-situ cracking behaviour by stress relaxation. Unexpected drying cracking within the test specimens, attributed to less than optimal mix design, complicated creep measurements but the data suggests specific creep rates are lower for IPCs than conventional concrete, thus negating the hypothesis. Testing of early age cracking susceptibility under restraint similarly did not show strong evidence for improved cracking resistance.

Measurements of shrinkage from the freshly mixed plastic state for a single IPC formulation using image analysis techniques suggest that autogenous volume change on hardening is of significantly greater magnitude than later drying shrinkage. The dependence of the phenomenon on mix formulation and any consequential detriment caused to subsequent serviceability needs to be verified.

Keywords

Inorganic, polymer concrete, creep, shrinkage, cracking, restraint, drying.

Contents

Page

Figures

Page

Tables

Page

1. INTRODUCTION

'Inorganic polymer' is the generic name for a broad class of x-ray amorphous materials, characteristically produced via the ambient temperature reaction of a finely divided alumino-silicate source with a high pH alkali silicate solution (Davidovits 1991). They are clearly differentiated from the more familiar alkali-activated slag cements, together with which they could be considered to mark the two extremes of a continuum, because the setting and hardening processes are dominated by the formation of chemical bonds rather than the physical intergrowth of calcium silicate hydrates. The resulting polymerised structure, consisting of tetrahedral Al – O units and more variably coordinated Si – O units with the alkali ions supplying charge balance (MacKenzie 2003), confers properties of moderate strength and hardness, good chemical resistance, and thermal stability to over 1000ºC. In this sense, inorganic polymers can be envisaged as analogous to ceramic materials but formed at low temperature.

Inorganic polymers have attracted considerable attention as an alternative to conventional Portland cement for use as a binder in construction. This derives both from their intrinsic attributes of chemical and fire resistance that offer the opportunity to enter markets inaccessible to conventional cement-based products and also, perhaps more significantly, from their potential environmental advantages. Unlike Portland cement, whose manufacture necessitates the high temperature decarbonisation of limestone, production of an inorganic polymer is an essentially low energy process with a relatively small greenhouse gas emissions footprint. On the basis of a life-cycle analysis, Gourley (2003) estimated that production of a tonne of inorganic polymer would generate 164 kg of CO_2; this is approximately one-sixth of the emissions for an equivalent mass of Portland cement (Alcorn 2003). A further synergistic benefit is that some industrial wastes and slags, particularly the fly-ash generated from coal combustion in power stations, are of suitable composition to supply the alumino-silicate feedstock.

Despite widespread recognition of the potential for IPC, the majority of the published literature focuses on the reaction chemistry and microstructure of the cementing phase, rather than the design properties of the resultant concrete. Knowledge of the latter is necessary to facilitate their use by engineers and drive the development of codes and standards.

1.1 Local developments

New Zealand can justly be said to be at the forefront of construction applications for inorganic polymer technology, through the efforts of researchers and practitioners at Industrial Research Limited and Golden Bay Cement. A notable achievement has been the development of methods to regulate the setting time of binders produced using Huntly power station fly-ash as the precursor material (Nicholson et al 2005). The extremely short setting times after activation formerly experienced with calcareous 'Class C' fly-ashes of this type had prevented their exploitation in this role worldwide.

Another significant accomplishment has been Golden Bay Cement's mastery of the process variables for large-scale production, to the point where IPCs can now be successfully batched and delivered using conventional ready-mix plant and equipment. It was observations made during the field trials this breakthrough permitted that prompted this study.

To demonstrate durability and general performance, an access track subject to light traffic and stock movements was laid in Whangarei using IPC. While the track employed continuous slab lengths of up to 12 m, unbroken by control joints, no shrinkage cracking has been observed (Warren South, personal communication, 16

October 2006). In contrast, a conventional concrete slab will typically crack at intervals of 2–4 m to relieve accumulated shrinkage stress, depending on the degree of restraint to which it is subjected.

1.2 Shrinkage, creep and relaxation

Concretes, whether produced with Portland cement or an inorganic polymer binder, share the salient feature that they are manufactured in a plastic state, with the desired flow achieved through the addition of water in excess of the stoichiometric requirement for the chemical reactions that produce stiffening and hardening. Consequently, they are porous materials and can be expected to suffer an induced isotropic compressive stress within the rigid binder phase when the excess water begins to evaporate. This hydrostatic tension, ordinarily expressed as shrinkage, develops in response to the formation of menisci within previously completely water-filled capillary pores (Mindess and Young 1981).

Given this similarity in nature, it is reasonable to ask why IPC should behave differently to conventional concrete. One possible answer relates to the phenomena of creep and relaxation.

Creep is formally defined as “the time-dependent increase in strain in a solid resulting from force” (ASTM E 6–07 *Standard terminology relating to methods of mechanical testing*). Virtually any material will undergo creep at some condition of loading. Nevertheless, creep in concrete is unusual because it is observed under normal service conditions and over a wide range of stress levels. Indeed, the creep of mature concrete is found to be linearly proportional to an imposed (compressive) stress up to approximately 50% of the concrete’s ultimate strength (Weiss 2006).

While analysis of concrete cracking is complicated by the many variables that may have an effect, the root cause is simply stated: concrete will crack when the accumulated stress, from restrained drying shrinkage for example, exceeds its tensile strength. The beneficial role in this played by creep is shown diagrammatically in Figure 1. Consider a freshly laid concrete slab (a) with a given initial length. Under ideal conditions, without any interference from the surrounding environment, unrestrained drying shrinkage will occur, giving the net reduction in length shown in (b). This occurrence is unrealistic in practice because slab movement will invariably be constrained to some degree, if only by friction of the underlying substrate. Consequently we suppose the hypothetical case of perfect restraint, which exactly preserves the initial dimensions of the slab. Achieving this situation requires imposing a fictitious load on the concrete to counteract the shrinkage stress (c). However, as a result of the applied load, the length of the slab will increase due to concrete creep (d). To maintain the condition of perfect restraint an opposing load is necessary (e), with the net result being a reduction in shrinkage stress experienced by the slab (f).

This discussion illustrates the significant role that creep can play in determining the magnitude of stresses that may develop in concrete, particularly at early ages. It has been estimated (Ross 1958) that stress relaxation due to creep may reduce stress by 30–70%. Thus, a reasonable explanation for reduced in-situ shrinkage cracking of IPC, relative to Portland cement concrete, is greater intrinsic creep, a hypothesis this report attempts to confirm.

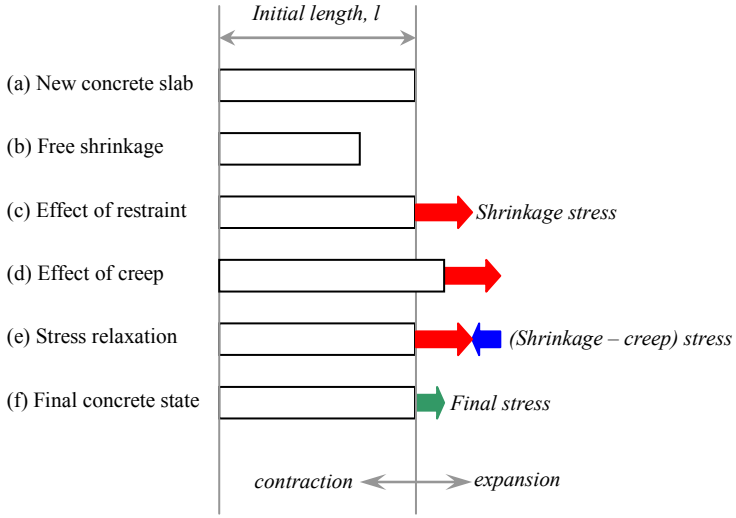

Figure 1: Schematic description of stress relaxation due to creep in a concrete slab (after Weiss 2006)

Neville (1995) has stated that the ability of creep to equalise or relieve stress concentrations has "contributed very considerably to the success of concrete as a structural material". Despite this, it is not necessarily desirable that IPC should prove to possess significantly greater creep; too high a rate could lead to problems with excessive deflection of elements under load. It could also increase the difficulty of achieving satisfactory pre-stressing and post-tensioning.

1.3 Project aims

To compare the creep, cracking susceptibility, and early age shrinkage of IPCs with an analogous standard structural concrete with a view to explaining field observations of superior performance.

2. SAMPLE PRODUCTION

Five distinct concrete mix designs were selected for study in consultation with Golden Bay Cement. These consisted of a conventional 32.5 MPa grade structural concrete, an IPC of similar strength utilising Class C Huntly fly-ash as the precursor material, and three IPC formulations of varying strength derived from imported Australian Class F Gladstone fly-ash. Mix descriptions, and the codes by which each are referred to throughout this report, are given in Table 1.

A grade D sodium silicate solution (Na_2O 14.7%; SiO_2 29.4%) and industrial grade concentrated sodium hydroxide and/or potassium hydroxide solutions were used to activate the IPC mixes. The mix formulations are proprietary to Golden Bay Cement and commercially sensitive so further details are not provided in this report.

Standard concrete aggregates, consisting of 19 mm and 14 mm greywacke chip, PAP7 manufactured sand and fine natural dune sand, were used for all the concretes. The estimated volumetric proportions of each aggregate per mix are shown in Figure 2. Of particular note is that the HFA (Huntly fly-ash) IPC uses an essentially identical aggregate skeleton to the conventional Control mix, whereas all the GFA (Gladstone) mixes lack the coarse sand fraction. Of the latter mixes, the volume ratio of aggregate to inorganic polymer binder decreases with increases in the nominal strength of the mix and ranges from 72% (GFA 20) to 67% (GFA 60).

Table 1: Formulations of the concrete mixes investigated

Mix code	Nominal compressive strength (MPa)	Binder type
Control	32.5	Golden Bay type GP Portland cement
HFA	35	Alkali sodium silicate-activated Huntly Class C fly-ash (NZ) and ground granulated blast-furnace slag
GFA 20	20	Alkali sodium silicate-activated Gladstone Class F fly-ash (Australia) and LG slag
GFA 45	45	
GFA 60	60	

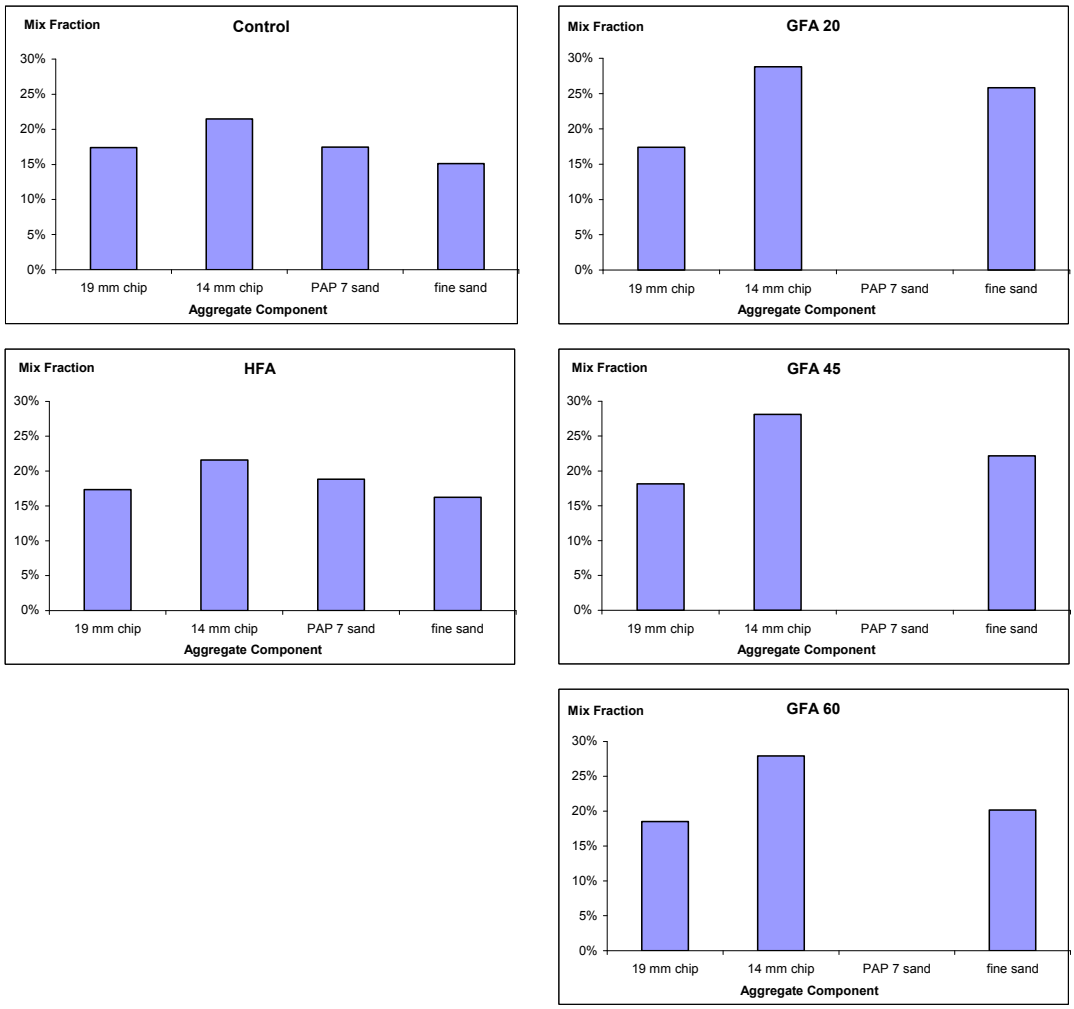

Figure 2: Volume fractions of the various aggregate components incorporated in each mix

Each test mix was produced as a single 70 L batch at BRANZ's Judgeford laboratory using a 100 L capacity pan mixer with a rotating bowl and offset rotating paddles. The mixing procedure for the IPCs was similar to that for a conventional concrete, involving blending the aggregates at a known moisture content above SSD (saturated surface dry) condition, introducing the other solid materials, and finally adding the alkali activators plus water as required. Typical mixing times were around five minutes, including an intermediate two minute standing time.

After mixing, appropriately sized test specimens were cast into steel moulds using standard compaction and finishing techniques, and the hardened concrete was stripped out after 24 hours. The one point of difference in handling of the IPC specimens related to curing: Jason Goile (personal communication, 2006) advised that standard curing by immersion in water was not recommended, and that Golden Bay adopted no special alternative procedure, generally leaving demoulded specimens under ambient laboratory conditions.

For the purposes of this study, care was taken to protect the specimens against drying during the period between casting and testing. Polythene sheet was used to cover any exposed trowelled faces after casting; the stripped IPC specimens were sealed into plastic bags immediately on demoulding and stored in closed plastic containers at 21ºC until required. Control concrete samples were cured as normal, in a fog room complying with the requirements of NZS 3112: Part 2:1986 *Methods of test for concrete – Tests relating to the determination of strength of concrete*.

3. RESTRAINED RING TESTING

To compare the relative susceptibility of the IPC and Control mixes to cracking, experiments were carried out in accordance with ASTM C 1581–04 *Standard test method for determining age at cracking and induced tensile strength characteristics of mortar and concrete under restrained shrinkage*. The principle of the test is simple: a concrete ring is cast around a stiff core that provides restraint. If the concrete shrinks, for whatever reason, tensile tangential stresses are developed in the ring and may lead to cracking. When or whether this occurs depends primarily on the interplay of the particular mix's properties of shrinkage potential and rate, tensile strength development, and creep relaxation.

To perform the test, 40 mm thick annular concrete specimens were cast around a 150 mm high restraining ring fashioned from 330 mm diameter structural steel pipe with a 13 mm wall thickness and polished on both faces. Concentrically mounting the restraining ring inside a removable cardboard 'formatube' outer wall, on a baseplate lined with Teflon to minimise friction, completed the mould. A completed example is shown in Figure 3.

The inner surface of the restraining ring was instrumented with electrical resistance strain gauges, which permitted the build-up of stress due to the concrete shrinking and the timing of any relief through cracking to be monitored. Four 120Ω foil-type bonded strain gauges with a gauge factor of 2.1 were installed per ring, equally spaced at a mid-height position and in a radial orientation. Each gauge was independently wired as one leg of a Wheatstone bridge. Two precision wire-wound 1 kΩ resistors plus an unstressed strain gauge to provide temperature compensation completed the quarter bridge circuit. Resulting strain measurements were captured at five minute intervals using a high precision Agilent 34970A data acquisition unit.

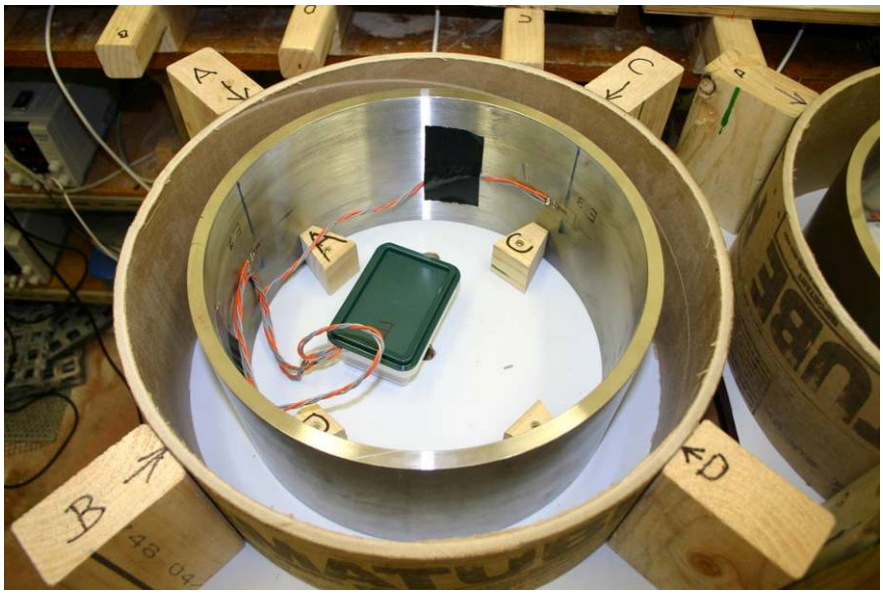

Figure 3: Formwork for a restrained ring specimen prior to casting

Due to the limited width of the annular space between the inner and outer walls of the mould, the plastic concrete mixes were sieved to remove aggregates with a nominal aggregate size greater than 13 mm prior to casting. The moulds were filled in two layers, compacted using a vibrating table, and the exposed surface struck-off and finished with the minimum trowelling necessary to achieve a flat surface.

Immediately after casting the specimens (two replicates per mix) were transferred to a temperature and humidity controlled environment maintained at 23±2°C and 50±5% RH and data logging commenced. For the first 24 hours, the concrete was protected from moisture loss by polythene sheeting. Subsequent to this point, the 'formatube' outer wall and the fastening devices locating the steel ring on the base were removed and the top (trowelled) face of the concrete sealed with molten paraffin wax (Figure 4). This helped restrict subsequent moisture loss to the circumferential surface, ensuring a more uniform distribution of shrinkage stress.

Figure 4: 20 GFA ring specimen after stripping

Figure 5 illustrates typical examples of the developed strain recorded in the steel rings after casting. A variety of behaviours are observed, depending on the concrete type. The Control behaves as expected, with significant stress only beginning to accumulate 24 hours after casting when curing is stopped, the mould wall has been removed, and drying commences. The stress rises smoothly to a peak, at which point a significant and rapid unloading event occurs. This event coincided with the visual observation of one or more full wall thickness longitudinal cracks in the concrete ring (Figure 6), indicating that the drying shrinkage stress had exceeded the tensile strength of the concrete.

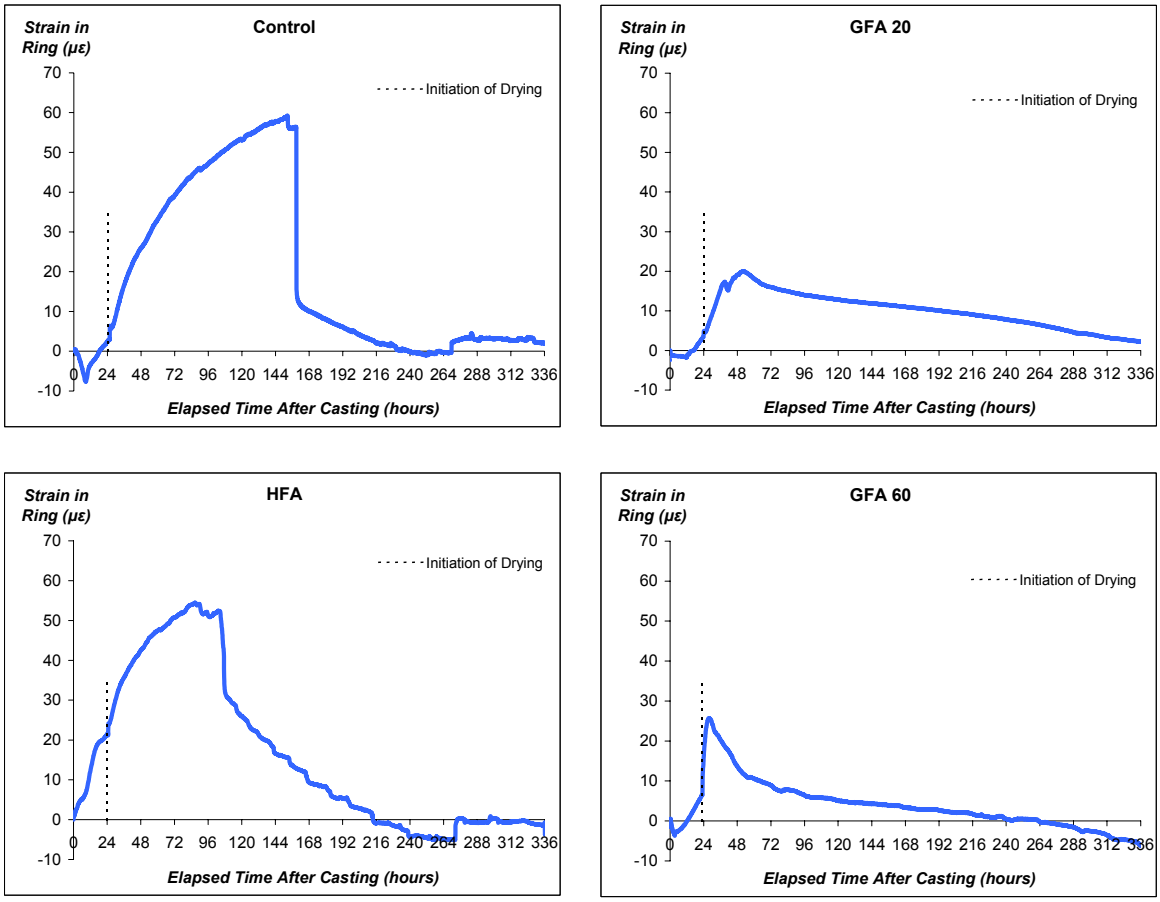

Figure 5: Strain development in 'restrained ring' specimens

In contrast, the GFA specimens induced a far lower stress in the steel restraining ring, which diminished gradually with time from a peak 30–60 hours after casting rather than being relieved in a single event. This relief appeared to arise from a comparatively fine-grained network of 'map' or 'pattern' cracks developed on the circumferential drying surface, with a slight preferential crack orientation to the longitudinal axis of the ring. The cracking was more obvious in the GFA 60 specimens than the GFA 20 specimens; the GFA 45 mix was not tested due to the limited number of instrumented restraining rings available. Photographs of typical crack patterns are shown in Figure 7.

Figure 6: Control concrete restrained ring specimen, showing full wall thickness longitudinal crack

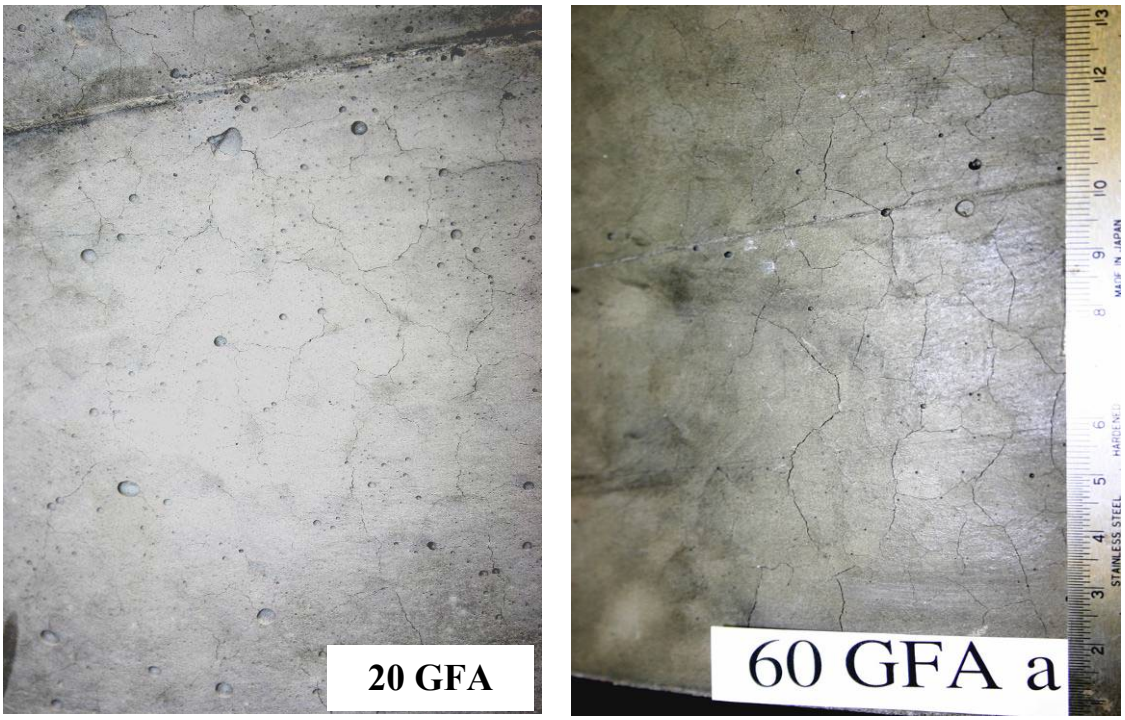

Figure 7: Fine-grained pattern cracking observed in the circumferential wall of GFA IPC specimens

The performance of the HFA rings more closely resembled that of the Control specimens than the other IPCs, developing a similar stress level and relieving the majority of stress in a single crack event. However, the primary longitudinal cracks were less well-defined than with the Control. It was also not obvious from visual examination that they extended through the full thickness of the ring wall, which may explain why some stress remained in the rings after cracking. Fine pattern cracking reminiscent of that of the GFA mixes was also observed, albeit developed to a lesser extent. Interestingly, there is some suggestion in the strain gauge data that significant shrinkage occurred prior to the initiation of drying.

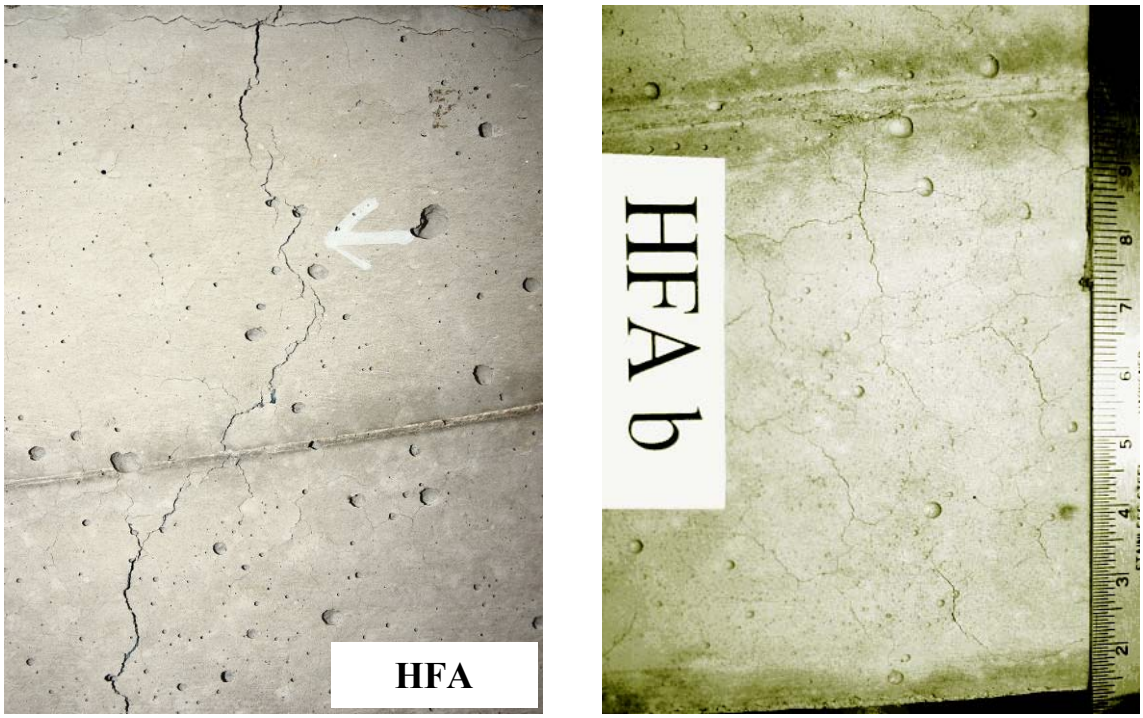

Figure 8: Crack patterns in the HFA specimens – a primary longitudinal crack (left) and pattern cracking (right)

A comparison of the average restrained ring results for the different mixes is presented in Table 2. On the basis of the extensive network of cracking in the GFA mixes and the similar peak strain and early cracking time of the HFA relative to the Control, these particular results do little to support the contention that IPCs have a lower tensile cracking susceptibility than conventional concrete. More work is recommended to understand this result.

Table 2: Summary of behaviour in 'restrained ring' test specimens

Mix	**Peak strain** (microstrain)	**Time of strain relief** (hours)	**Observed crack patterns**
Control	59	159	Longitudinal full-wall thickness crack visible in specimens after 7 days
HFA	54	105	Longitudinal partial thickness crack visible on 4th day plus some pattern cracking
GFA 20	20	No discrete relief event	Fine pattern cracking visible on 5th day
GFA 60	25	No discrete relief event	Extensive fine pattern cracking visible after 4 days

4. SHRINKAGE MEASUREMENT

While creep mediates its effect, the extent of shrinkage is the driving force for early age cracking. In a Portland cement concrete, three distinctive mechanisms have been identified as giving rise to this: chemical shrinkage, self-desiccation and drying shrinkage. Very briefly, chemical shrinkage arises from the volume difference between the hardened cement phase and the equivalent quantity of un-hydrated cement and water needed to produce it, self-desiccation is a consequence of the removal of water from capillary pores due to the hydration of hitherto un-reacted cement, and drying shrinkage is moisture loss to the external environment from vapour pressure differences (Neville 1995).

Routine techniques for the measurement of concrete shrinkage generally capture only the drying component of these mechanisms because they require physical measurements to be made across cast-in gauge points. This necessities a level of robustness in the sample and hence cannot commence until the concrete has hardened. An alternative is to embed strain transducers in the fresh concrete, which can be monitored from the point of casting. However very early age shrinkage occurring prior to the initial setting time may not be accurately recorded due to the inherent stiffness of the strain gauges.

In practice, measuring only drying shrinkage is of little consequence because its magnitude significantly exceeds the other phenomena, except where the concrete is batched at extremely low water-to-cement ratios. Whether this assumption is also true for IPCs is examined in the work described by this section.

4.1 Image analysis

To allow measurement of shrinkage from immediately after casting, the common image processing technique of particle tracking was adopted, in which movement of a chosen target is tracked across a chronological series of time-lapsed digital images taken in a fixed frame of reference. Routine use of this technique has been facilitated with the availability of commercial software for simple and accurate analysis of digital images and the improved quality and resolution of CCD sensors in low cost ‘consumer grade’ digital cameras. Gary Ong and Myint-Lay (2006) have recently demonstrated the application of this technique to monitoring the shrinkage of cementitious materials, and this method was exploited here.

For the experiment, samples of the Control and HFA mixes were cast in 500x100x100 mm steel beam moulds that had been lined with Teflon sheet to minimise friction; the available camera field-of-view prevented inclusion of the other IPC formulations. Immediately after casting the beams were placed in a controlled drying environment of 23±2°C and 50±5% RH and three pairs of imaging targets were inserted into the freshly trowelled surface of each beam, approximately 400 mm apart, as illustrated by Figure 9. The targets followed the design of Gary Ong and Myint-Lay (2006) and comprised a 100 mm long x 0.5 mm diameter wire topped with a ca. 15 mm diameter white plastic disc. Laser printed on the centre of each disc was a black 4x4 mm square. The inserted pins penetrated the full depth of the beam section to prevent settlement of the disc into the concrete surface. It is a reasonable assumption that any movement of the concrete as it shrinks will be reflected by a corresponding change in the tracked position of the reference pin.

Figure 9: Example of the digital images captured for early age shrinkage analysis, showing the reference targets installed in the beam specimens

A digital SLR camera with a 6 megapixel (3072 x 2048) hardware resolution was rigidly fixed a distance of 1 m above the specimens and perpendicular to the trowelled face of the two beams, which filled the camera's field of view. PC control of the camera allowed images to be taken at specified intervals and archived for later analysis. Images were captured from 0.5 hours after casting of the first beam, with an initial sampling frequency of one image every two hours.

To track movement of the reference pins across the chronological sequence of images, the captured digital files were first re-sampled at the higher resolution of 6144x4096 pixels to increase the sensitivity of the analysis, by employing a bicubic interpolation procedure. The re-sized images were then segmentation thresholded for conversion from colour to high contrast black and white. This allowed the target points to be clearly distinguished from the background of the trowelled specimen faces (Figure 10), which is a necessity for convenient analysis.

The pixel coordinates of each 4 mm black target in the resulting binary image were then derived using a 'blob analysis' software routine. This delineates the target outline based on changes in pixel values, which are now restricted to black or white, and calculates its geometric centre. By dividing the change in distance between each pair of points and the gauge length (the number of pixels separating them in the first image) the current shrinkage strain could be obtained.

An example of the collected data for two paired reference pins over a 24 hour period is shown in Figure 11. As expected the majority of movement is along the *x*-coordinate, which corresponds to the longitudinal axis of the beam. The 'saw teeth' in the curve are noise in the digital images, most probably arising from changes in light intensity of slight perturbations of camera position. In theory, the software used could distinguish position changes of $<10^{-3}$ of a pixel, corresponding to 0.2 microstrain over the 5000-pixel distance that represented the 400 mm gauge length between pins. In practice, fluctuations due to noise reduce this sensitivity to approximately 20 microstrain.

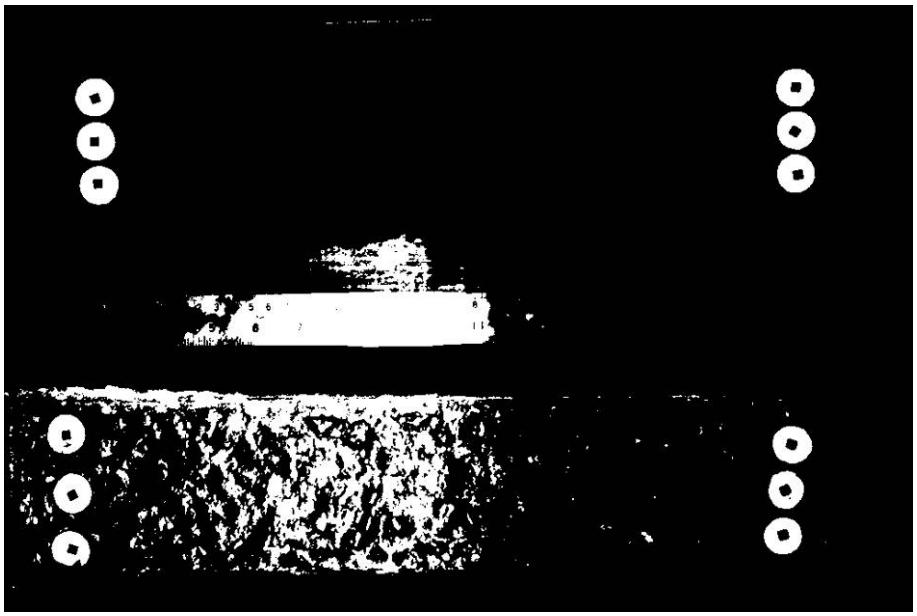

Figure 10: Image from Figure 9 after binary thresholding to distinguish reference targets from the specimen background

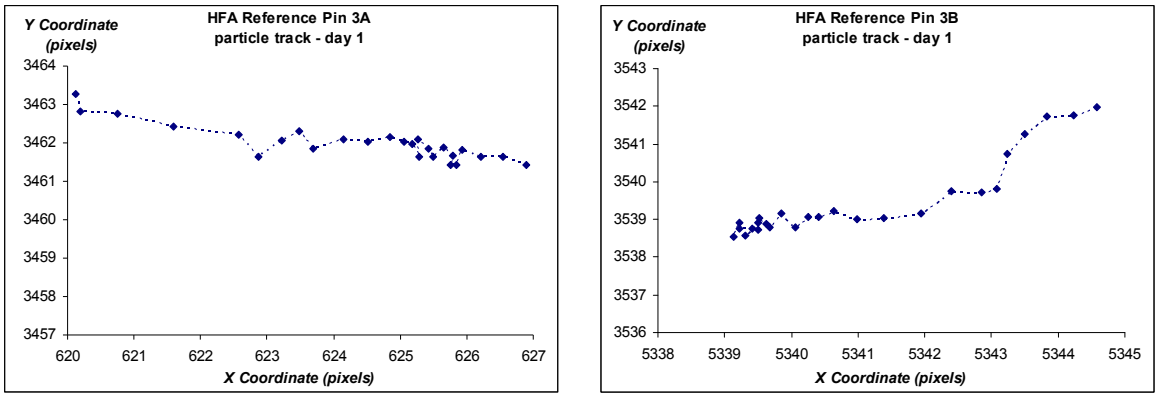

Figure 11: Location tracking of two paired reference pins embedded in the HFA beam over the time interval 0.5 – 24 hours after casting

Figure 12 illustrates the measured strain for each specimen in the hours immediately after casting. Two days worth of data are presented for the Control concrete; regrettably a disruption to the experiment lighting means only the first 24 hours are available for the HFA IPC. Nevertheless it is still clear that the very early shrinkage behaviour of the two concretes is quite dissimilar. The conventional concrete demonstrates an initial dilation of the distance between the reference pins, possibly a thermal effect related to the heat of hydration of the Portland cement. This is not reversed until after the onset of initial set, and even at 48 hours after casting there is little net shrinkage. By contrast, the HFA mix appears to begin shrinking even while still in the plastic state, and has reached 2,000 microstrain after 12 hours, at which point a marked change in the rate of shrinkage occurs. Speculatively this may reflect a change in the shrinkage mechanism or a structural change in the hardening binder. Irrespective of this, it is evident that 'chemical shrinkage' may be of larger magnitude in IPCs than conventional ones.

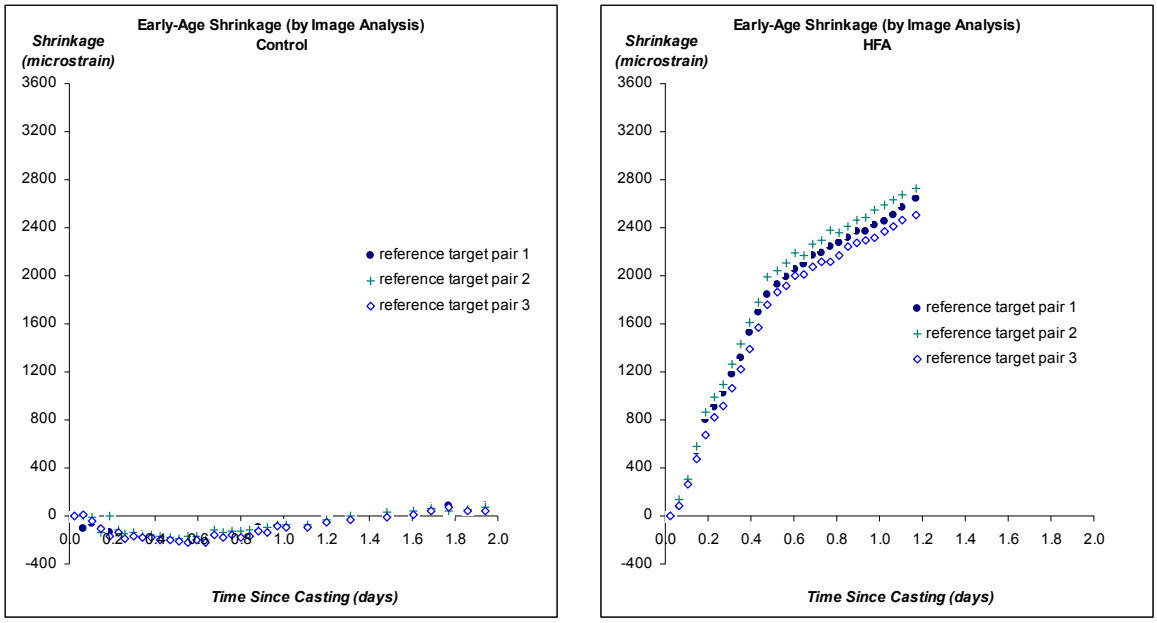

Figure 12: Early age shrinkage of Control concrete (left) and HFA IPC (right) determined by digital images captured in a chronological sequence

Figure 13 extends the dataset to 40 days. It is apparent that while the total extent of the HFA shrinkage is very much larger than that of the Control the majority occurs within the first week after casting. This would potentially be missed if measurements commenced after the concrete was allowed to harden.

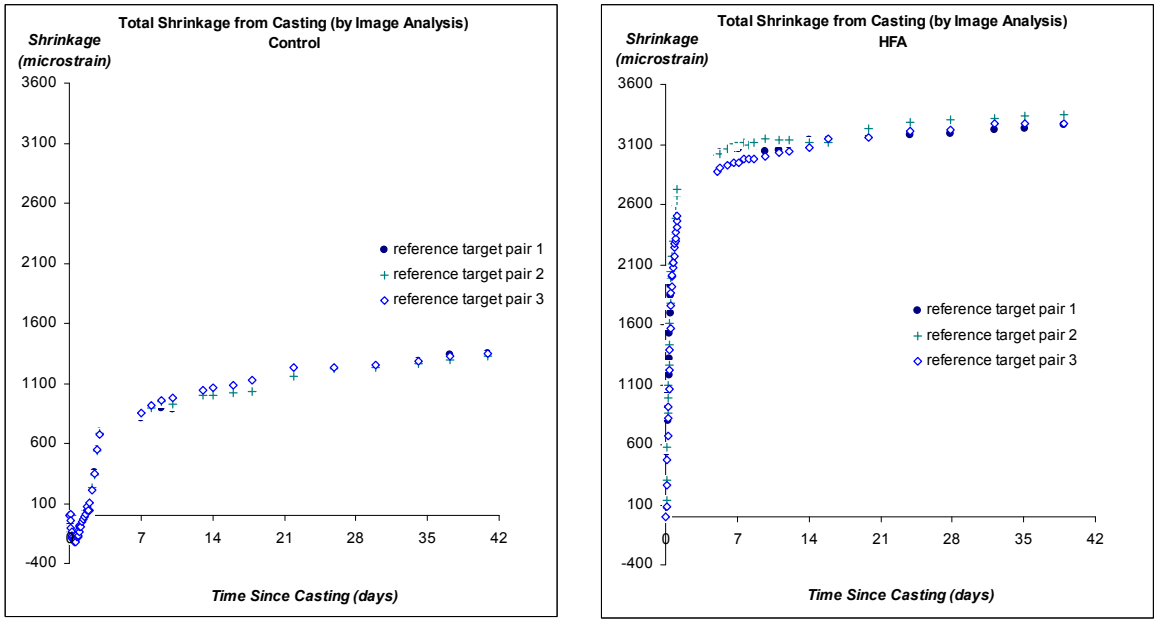

Figure 13: Shrinkage measured by digital image analysis up to 40 days from casting

It is acknowledged that the measurement technique presented here is novel, and of relatively untested calibration. As a rough check on the validity of the results, the following points are noted. First, the shrinkage of the Control mix at 1,350 microstrain, while a little higher than might be expected for a 32.5 MPa crushed aggregate concrete, is not unfeasible considering that the beam received no curing. Gary Ong and Myint-Lay (2006) also state that because loss of water primarily occurs through the

exposed trowelled face it will shrink somewhat more than parts of the specimen nearer the base of the mould. If this differential develops, the reference pins may correspondingly incline slightly from the vertical, the net effect being to slightly exaggerate the measured movement, which should be considered as an upper bound. Secondly, the final shrinkage of the HFA of 3,300 microstrain equates to approximately 1.6 mm across the full length of the 500 mm beam. This was comparable with the cumulative size of the visually observable gaps created by movement of the hardened concrete away from the end walls of the mould.

4.2 AS 1012.13 Drying shrinkage measurements

For comparative purposes, Figure 14 illustrates the shrinkage of the various mixtures measured using AS 1012.13 – 1992 *Methods of test for concrete. Method 13: Determination of the drying shrinkage of concrete for samples prepared in the field or in the laboratory*. Note that this method specifies that test prisms, with cast-in gauge studs, are allowed to harden for 7 days protected from water loss before being placed in the 23±2°C and 50±5% RH drying environment where a 'zero' reading is made. Thus the origin of the Figure 14 graphs is a week after casting and much of the potential IPC shrinkage identified in the preceding section may have been missed. As might be expected from the later portion of Figure 13, the measured Control drying shrinkage after 56 days drying (Table 3) exceeds that of the HFA IPC. The drying shrinkage of the GFA mixes varies from 550 to 920 microstrain; this possibly reflects the competing influences of paste to aggregate volume and developed inorganic polymer strength.

Table 3: Summary of AS 1012.13 concrete drying shrinkage results

Mix code	**Mean 56 day shrinkage** (microstrain)
Control	840
HFA	520
GFA 60	720
GFA 45	920
GFA 20	550

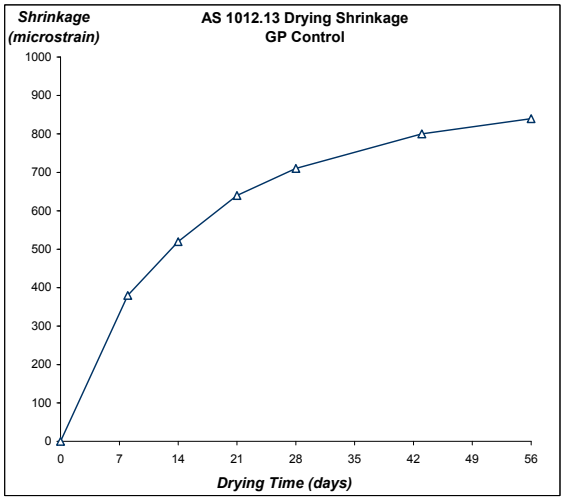

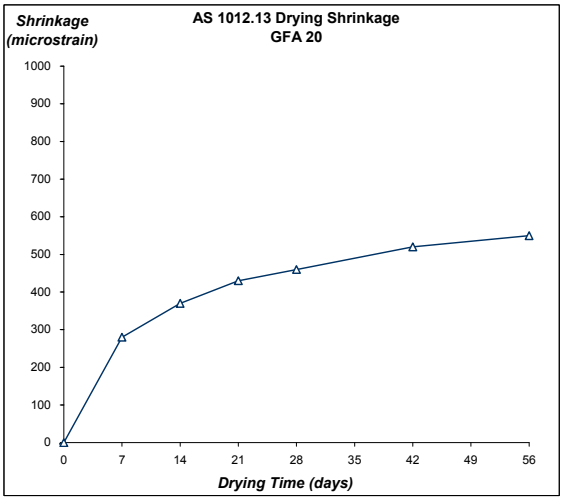

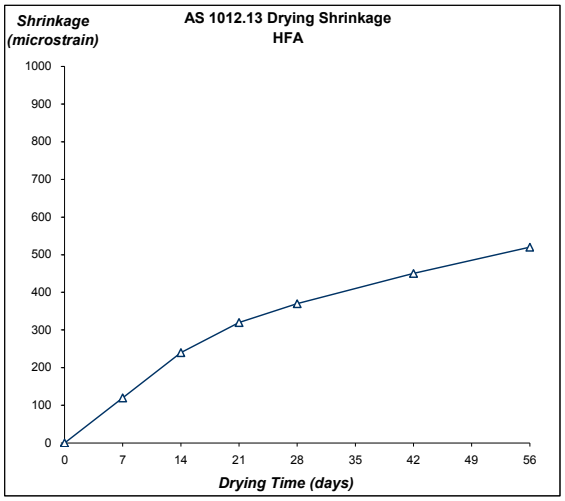

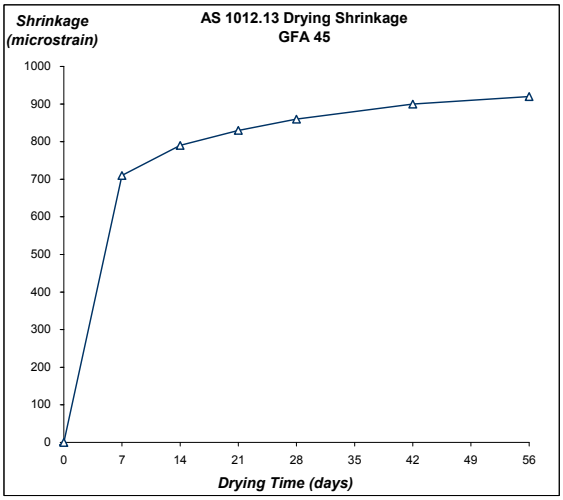

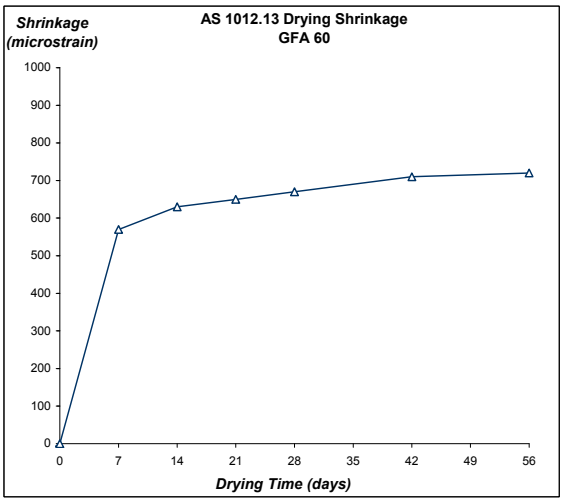

Figure 14: AS 1012.13 concrete drying shrinkage results

5. CREEP TESTING

For true fidelity to the scenario of IPC shrinkage crack being mitigated by stress relaxation discussed in Section 1.2, the property of tensile creep would ideally be measured. This procedure is made difficult by the comparatively low tensile strength of concrete, but a wide variety of possible solutions have been proposed. These include the simple uniaxial loading of specimens through a dead weight attached to a lever arm (Bissonette and Pigeon 1995), and more complex apparatus using pressurised cylinders to apply a constant load to the inner surface of a hollow concrete cylinder (Ross 1954). However, in the absence of a standardised test method, and considering the relative paucity of comparative data for performance in tension, the decision was made to carry out conventional creep testing during which the concrete is under compression.

The creep of mass concrete in uniaxial tension is normally assumed to be 20–30% higher than for loading under a compressive stress of equal magnitude, with similarly shaped curves for the evolution of creep strain with time (Neville 1995). There is a consensus of opinion that the exact difference depends on age at loading and tensile creep may be significantly greater in dry conditions at early ages, although sufficient contradictory evidence exists to prevent definitive statements about the relationship being made.

Creep testing of the Control and IPC mixes was conducted on standard 200 x 100 mm diameter test cylinders in accordance with AS 1012.19 – 1996 *Determination of creep of concrete cylinders in compression*. A number of deviations from the stated method were made with regard to the curing and conditioning of test specimens. As noted previously, Golden Bay recommends against standard moist curing of IPC cylinders; consequently these specimens were simply sealed in plastic bags and stored at 21ºC to 7 days of age.

Due to delays in the construction of appropriate creep rigs, the duration of the subsequent conditioning at 23±2°C and 50±5% RH was also extended until 56 days after casting, rather than the specified 28 days. Because a compensating value for any free drying shrinkage is routinely subtracted from the total measured strain when calculating the load-induced creep in the course of the test, this delay was considered to be of minor consequence.

An enhancement to the standard procedure was the inclusion of additional samples for determining the influence of moisture boundary conditions on creep of the IPCs. Measuring ‘basic creep’, as described in ASTM C 512 – 02 *Standard test method for creep of concrete in compressio*n, in addition to ‘total load-induced creep’, achieved this aim. These test cylinders were protected against gain or loss of water over the entire conditioning and test period by enclosing in a moisture-proof jacket of self-adhesive butyl rubber sheet after fabrication. In the graphs and tables that follow, these specimens are referred to as ‘sealed’, whilst the standard specimens are referred to as ‘exposed’. The various permutations of specimen treatment are summarised in Table 4.

To subject the test concretes to sustained compressive loads, five conventional design spring-loaded reaction frames were constructed, as pictured in Figure 15. One reaction frame was dedicated to each mix and contained two ‘exposed’ and two ‘sealed’ specimens mounted in a column, with a spherical seat at the column base to help ensure axial loading. To this purpose the ends of test cylinders were also carefully ground to meet the planeness and perpendicularity tolerances specified by AS 1012.19. The initial stress was applied with a portable 25 tonne hydraulic jack in conjunction with a calibrated load cell, and each frame was equipped with four nests of concentric springs with a combined force constant of 5,250 N/mm to maintain the

stress. The concrete was stressed at 40% of the measured compressive strength of the 'exposed' specimens at time of loading and the frames located in a stable controlled environment room at 23±2°C and 50±5% R.H.

Table 4: Permutations of samples and initial conditioning for creep tests

Concrete type	**Specimen type**	**Initial curing received** (24 hrs – 7 days of age)	**Pre-test conditioning** (7 days – 56 days of age)
IPCs	Exposed	Sealed in plastic bags and stored at 21ºC	23±2°C and 50±5% RH
	Sealed	Sealed in plastic bags and stored at 21ºC	Butyl rubber moisture-proof jacket
Control	Exposed	Moist-cured at 21ºC	23±2°C and 50±5% RH
	Sealed	Moist-cured at 21ºC	Butyl rubber moisture-proof jacket

Figure 15: Creep testing rigs – load being applied with hydraulic jack (left) and induced strain being measured (right) with a Demec gauge (right)

To ascertain creep, the longitudinal strain induced in the loaded cylinders was measured with a demountable strain (Demec) gauge accurate to ±10 microstrain over the chosen 100 mm gauge length. The necessary gauge reference points were pre-epoxied to the specimens in four measurement lines, evenly positioned around the circumference of the cylinder at mid-height.

A corresponding series of unloaded 'dummy' cylinders were maintained beside each creep rig under the same environmental conditions (Figure 16). Measurement of strain in these specimens served as a control to indicate, and compensate for, any deformation experienced by the concrete because of causes other than load.

Figure 16: Unloaded 'dummy' cylinders, kept and measured to compensate for any deformation due to sources other than load

To date, the creep strain of the test concretes has been measured out to 28 days after loading, at daily intervals for the first week, and then weekly. Subsequent measurements will be taken monthly until discontinuation of the experiment. Figure 17 illustrates the strain-time histories due to basic and total load-induced creep for the various mixes. These creep strains are calculated from the difference between the average deformation in the loaded and unloaded dummy samples of each concrete, using the 'exposed' and 'sealed' specimens respectively.

It is frequently assumed that creep strains are linearly related to the applied stress, at least up to 50% of the ultimate compressive strength of the concrete (Mindess and Young 1981). Consequently it is valid and useful to introduce the concept of 'specific creep' to compare the performance of the various concrete types, which are loaded at different stress levels:

$$Specific\ creep, \phi = \frac{\varepsilon_{cr}}{\sigma}$$

where ε_{cr} is the creep strain and σ the applied load (usually in MPa). The accumulation of creep strain over a period of sustained loading has been found to have an approximately logarithmic relationship with time, linked by a proportionality constant known as the 'creep rate'. The creep rate is derived from the following empirical equation (AS 1012.19), which allows specific creep at any time to be estimated:

$$\phi = \left(\frac{1}{E}\right) + F(K) \cdot \log_e(t+1)$$

where t is the loaded time in days, $F(K)$ is the creep rate, and E is the instantaneous elastic modulus of the concrete on initial loading (i.e. load stress divided by immediately induced strain). Figure 18 plots the specific creep of the mixes against time on logarithmic scale; the slope of the lines yield $F(K)$ and the intercept E.

The measured parameters for basic and total specific creep at 28 days, creep rates, and the instantaneous elastic modulus for each of the concrete types are tabulated in Table 5.

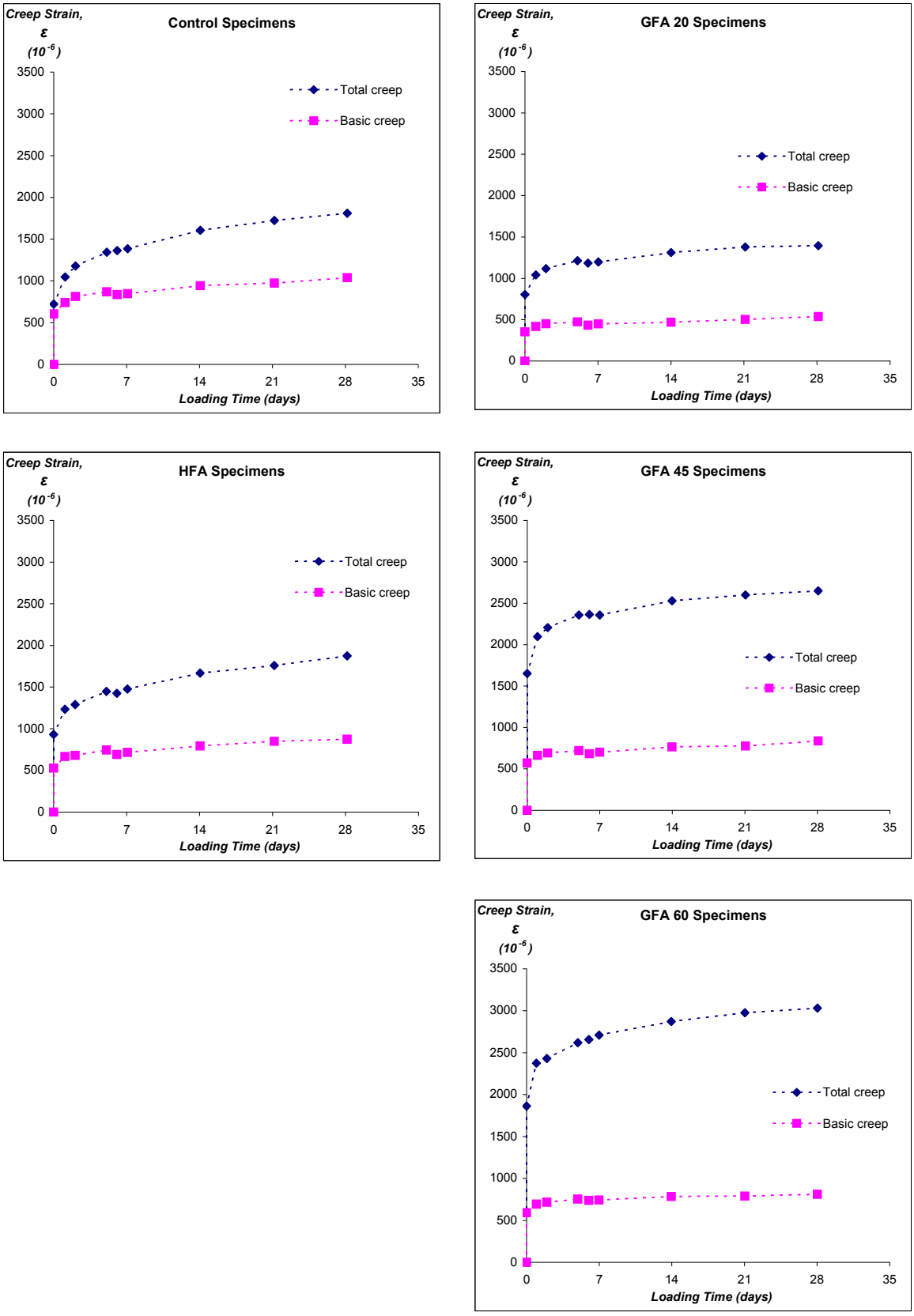

Figure 17: Total load-induced and basic creep strain development with loading time

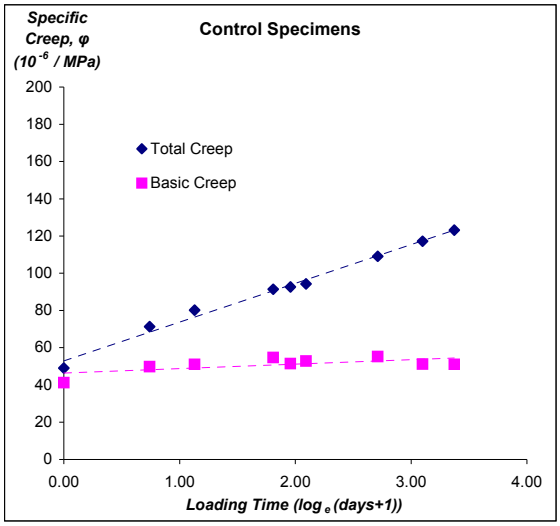

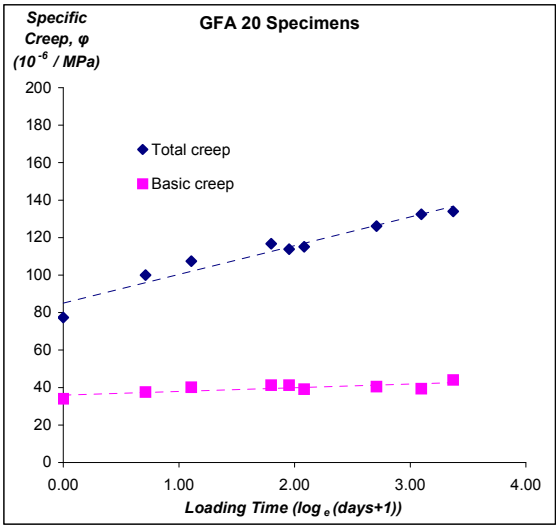

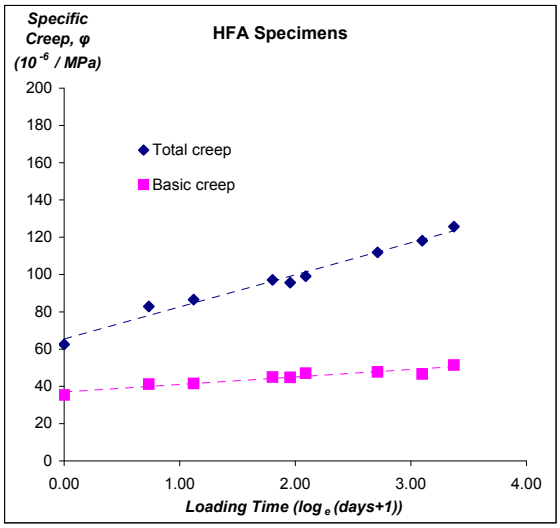

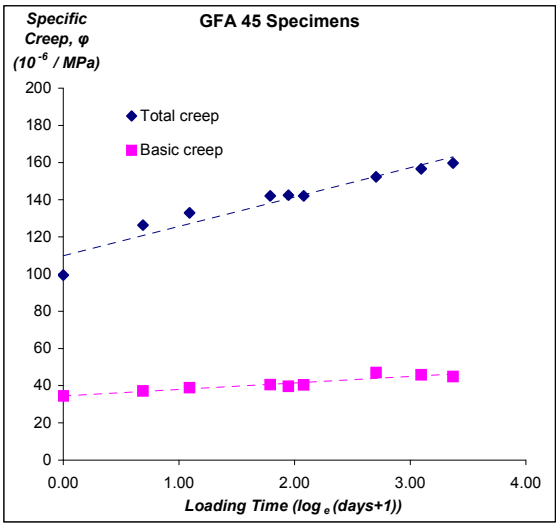

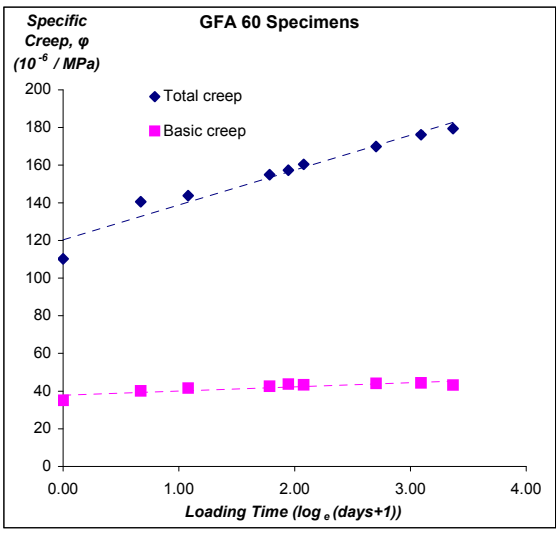

Figure 18: Development of specific creep (creep strain per MPa) with loading time

Table 5: Summary of creep testing results

Mix	Loading age (days)	Compressive strength (MPa)	Applied load (MPa)	Specimen treatment	Instantaneous elastic modulus, *E* (GPa)	Specific creep at 28 days, Φ (per MPa)	Creep rate, *F(K)*
Control	56	36.5	14.7	Exposed	20	123×10^{-06}	20.8×10^{-06}
				Sealed	24	51×10^{-06}	2.4×10^{-06}
HFA	56	37.0	14.9	Exposed	16	126×10^{-06}	17.2×10^{-06}
				Sealed	28	51×10^{-06}	4.0×10^{-06}
GFA 20	56	26.0	10.4	Exposed	13	134×10^{-06}	15.4×10^{-06}
				Sealed	29	44×10^{-06}	2.0×10^{-06}
GFA 45	56	41.5	16.6	Exposed	10	160×10^{-06}	15.8×10^{-06}
				Sealed	29	45×10^{-06}	3.5×10^{-06}
GFA 60	56	42.5	16.9	Exposed	9	179×10^{-06}	18.5×10^{-06}
				Sealed	29	43×10^{-06}	2.2×10^{-06}

One point is immediately apparent. The elastic response on initial loading of the samples differs significantly between those subjected to 'exposed' and 'sealed' conditioning. Figure 19 illustrated that all of the 'sealed' IPC specimens show a stiffer initial response than the Control mix. In contrast, the initial elastic moduli of the corresponding 'exposed' IPC specimens were very much lower. Only the Control concrete demonstrated initial loading responses of similar magnitude, suggesting the assumption that the differences in specimen treatment following initial curing would have a (comparatively) minor effect on their compressive strength was incorrect.

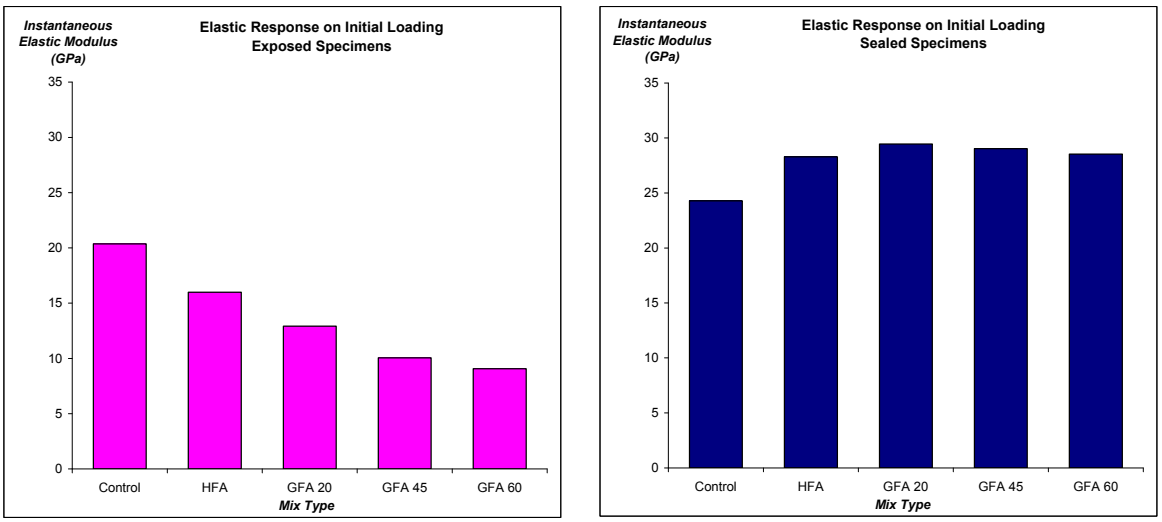

Figure 19: Elastic modulus measured on loading for exposed (left) and sealed (right) specimens

This was confirmed by sacrificing some of the dummy specimens to re-measure the compressive strength of the concretes, which was carried out 84 days after casting. As shown in Figure 20, the differences were found to be dramatic for the IPC mixes and, as might be expected, were similar to their variation in elastic response. The effect was much more pronounced for the GFA mixes than the HFA mix, and proportionally greater as the nominal strength of the GFA formulations increased. In contrast, the

strength difference in the Control mix is no more than would reasonably be attributed to more favourable conditions for ongoing cement hydration in the case of the 'sealed' specimens.

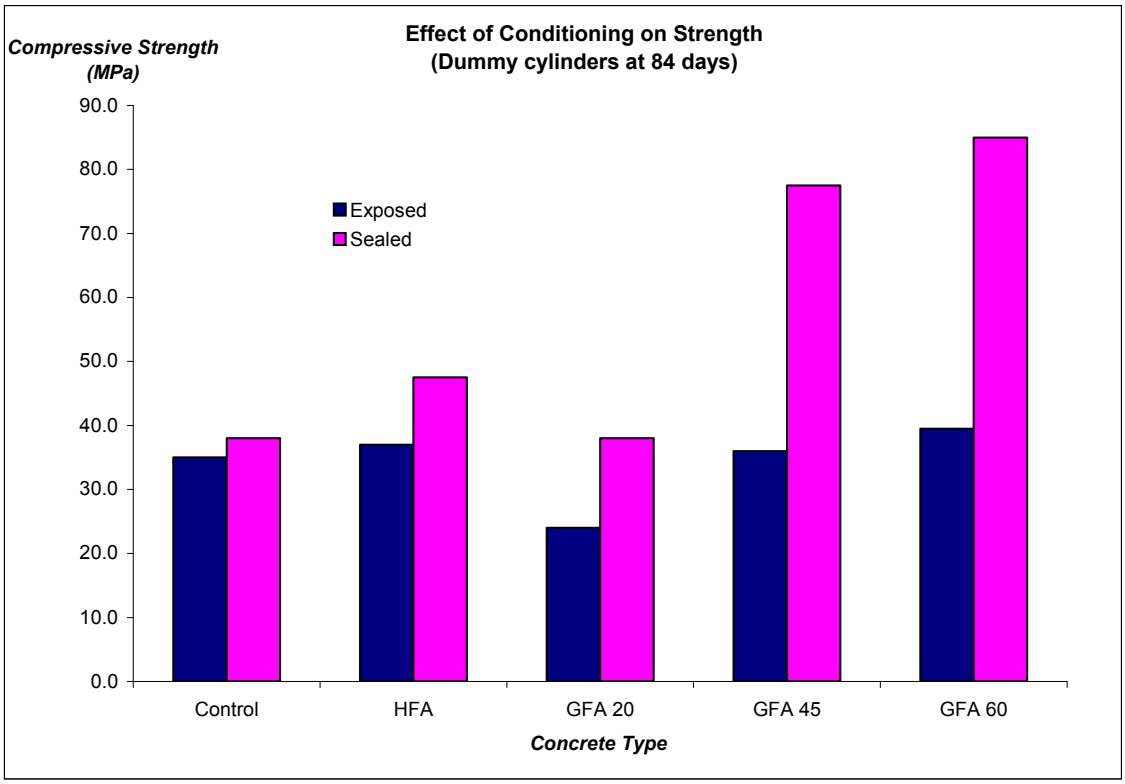

Figure 20: Discovered difference in compressive strength of dummy specimens due to storage conditions

The variation in strength with conditioning treatment appears to naively correlate with the extent of cracking visible on the surface of the dummy cylinders that received 'exposed' conditioning. A close visual examination suggested this cracking was quite pervasive amongst the IPC samples and, at least on the cylinder ends, quite deeply penetrating. Figure 21 shows photographs of a 60 GFA example specimen. The apparent severity and pattern of cracking was similar to that observed in the restrained ring tests, and was estimated to escalate as follows:

Control (none) < HFA (minor) < 20 GFA < 45 GFA < 60 GFA (significant)

A re-examination of the AS 1012.13 drying shrinkage beams confirmed that the IPC specimens had also developed comparable cracks; Figure 22, which is a photograph of the surfaces of an HFA and 60 GFA beam side-by-side, demonstrates the range of intensity. Note the photographed specimens have been rubbed with white chalk powder to highlight the cracking pattern.

Given that the beams and cylinders were free to shrink without interference, the only reasonable conclusion for this phenomenon is internal restraint caused by the exterior surfaces of the IPC specimens drying more quickly than the less exposed interior core, i.e. an analogue to plastic cracking, but in the hardened state.

Figure 21: Examples of cracking developed in a 60 GFA dummy cylinder subjected to 'exposed' conditioning and storage

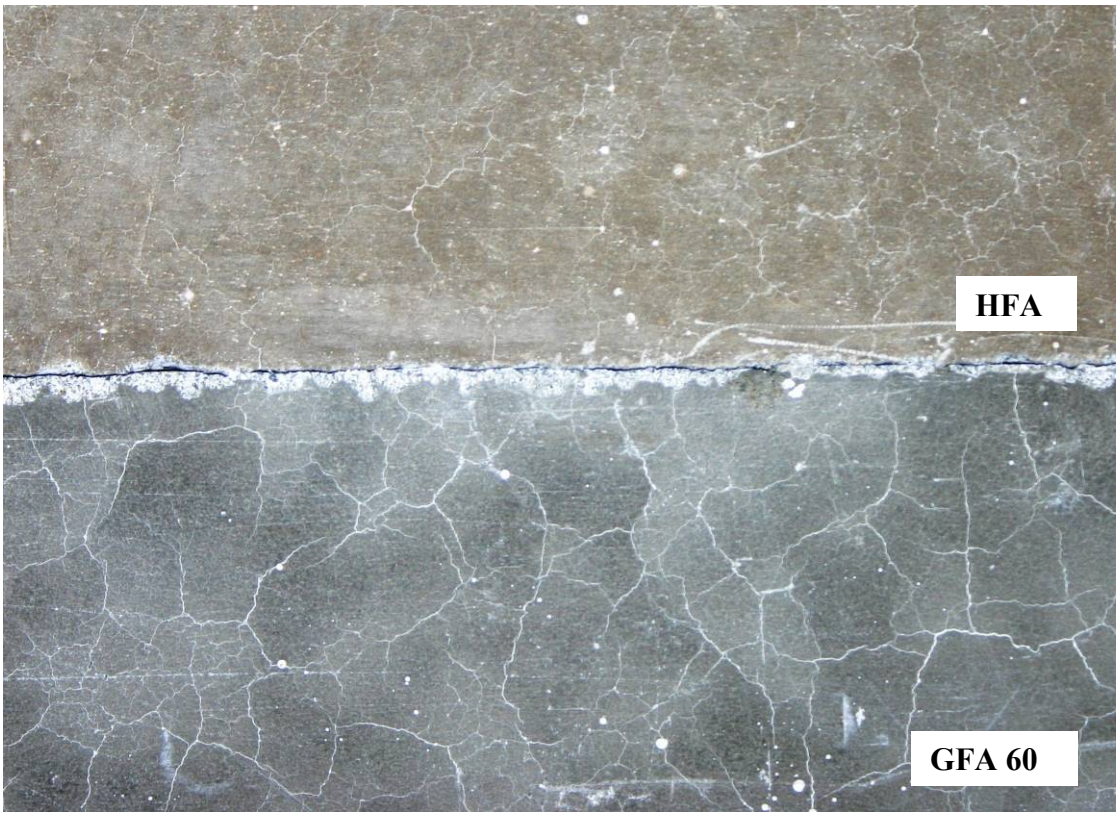

Figure 22: Examples of the range in severity of cracking observed in unrestrained AS 1012.13 drying shrinkage beams

Assuming that the 'sealed' specimens, which should have maintained a uniform moisture content, are not subject to this detrimental process, then their instantaneous elastic moduli (Figure 19) suggest that, at their maximum potential, the IPC mixes are uniformly stiffer than the Control concrete.

Cracking may not significantly affect the accumulation of creep strain after initial loading because the action of the compressive stress is to close them up. Figure 23 illustrates the determined creep rate, $F(K)$, of the mixes (i.e. the slope of the best-fit linear regression to the data presented in Figure 18). Irrespective of the differential influence of cracking it appears that, once loaded, the increase in specific creep with time for the 'exposed' IPCs is lower than for the Control mix. Taken in combination with the higher elastic modulus of the 'sealed' specimens, this seems to mitigate the hypothesis that creep relaxation is responsible for the absence of shrinkage cracks observed in IPC field trials.

Interestingly, the IPC specimens mimic the creep behaviour of conventional concretes in their dependence on moisture boundary conditions i.e. the total load-induced creep is significantly greater than the basic creep for a particular mix. Because total load-induced creep is already adjusted for any free drying shrinkage by subtracting strain development in the dummy specimens, the difference reflects a real increase in the magnitude of the creep effect that is somehow facilitated by lower humidity within the IPC.

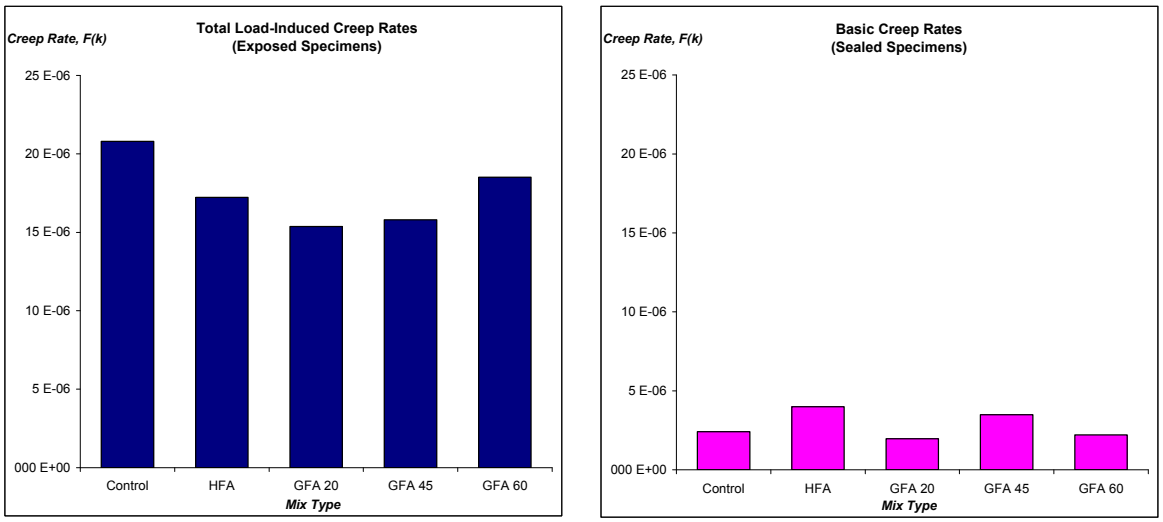

Figure 23: Comparison of total load-induced creep rate (left) and basic creep rate (right)

6. CONCLUSIONS

It is difficult to reach an unambiguous conclusion concerning the creep behaviour of IPC or its significance to relieving shrinkage stress. Many of the results discussed here appear to have been strongly influenced by the unconventional nature of the combined particle size distribution of the aggregates used in the GFA IPC mix designs.

It appears that inorganic polymers may have a very high early age shrinkage potential, and rate of shrinking, in the first one to two days after casting. This behaviour is in contrast to conventional concretes with the standard range of water-to-cement ratios, and presumably relates to autogenous volumetric change as the precursor materials dissolve and polymerise in the activating solution. The strain induced due to this effect appears to be significantly greater than that attributable to later age drying shrinkage. The magnitude of the latter phenomenon is comparable to that observed in a standard concrete.

It is uncertain whether this volume instability poses any practical detriment to the use or performance of IPCs. It seems plausible that the deformation is accommodated by similarly high levels of creep relaxation at this early stage in the hardening process. While the crack patterns observed in externally unrestrained samples of the IPC have been highlighted, particularly for their influence on instantaneous elastic modulus and compressive strength, they appear to largely derive from later drying shrinkage. Visible cracking, and reflection of its consequences in less than expected compressive strengths, was only observed on the specimens exposed to a reasonable aggressive 23ºC and 50% RH drying environment.

It is theorised that the GFA IPC specimens were so badly affected because in the absence of a coarse sand component, stress developed in the paste would be less effectively transferred into the aggregate skeleton, which ordinarily provides both restraint and a degree of stress delocalisation. Thus, stress gradients probably developed between the more quickly drying paste-rich surface of specimens and the more slowly drying and restrained interior, resulting in the tensile strength of the inorganic polymer binder being exceeded. This explains why cracking was most severely developed in the GFA 60 mix, which had the highest paste-to-aggregate ratio and also why the HFA mix, with a conventional concrete aggregate skeleton remained reasonably unaffected. However some minor cracking, which was totally absent from

the Control concrete, was still evident with this IPC formulation, suggesting further mix design refinement may be helpful.

Assuming that the HFA specimens do provide a relatively untainted representation of potential IPC performance, the question of why IPC slabs should display a reduced need for shrinkage control joints remains unanswered. Restrained ring testing suggests the HFA mix possesses a slightly increased cracking susceptibility relative to the Control, with the principal cracking event occurring two days earlier and at slightly lower stress levels. Furthermore, while the HFA has a lower instantaneous elastic modulus than the Control, it also possesses a lower total-load induced creep rate. Therefore the specific creep at 28 days is almost identical, providing little evidence of potential for enhanced stress relaxation.

It is recommended for future research that the highlighted apparent problem of mix design is separated from that of intrinsic inorganic polymer performance by initially studying only pure pastes rather than concretes. It is acknowledged that, as alumino-silicate sources themselves, aggregates cannot justifiably be regarded as chemically inert filler in an IPC. Nonetheless, it is difficult to understand the behaviour of a composite material without first comprehending that of its individual components.

A future programme should probably focus directly on early age tensile creep and creep development, rather than inference from standard compressive creep tests. Solutions for obtaining this from the strain accumulation in a restrained ring test have been derived (Attiogbe, See and Miltenberger 2001), but the calculation also requires accurate knowledge of free drying shrinkage rate and potential measured on specimens with the same exposed surface area to volume ratio as the ring, plus rates of tensile strength development. With IPCs it appears that careful account of autogenous shrinkage from casting would also be essential, necessitating dilatometer measurements on fresh paste samples under sealed conditions. It would also be interesting to know why the compressive creep of IPC and Portland cement concrete appear to be similar in demonstrating the same dependence on external moisture boundary conditions; perhaps the mechanism of internal movement of absorbed or intracrystalline water usually invoked to explain creep in hydrated calcium silicate cements also holds true for the quite different crystal structures proposed (Barbosa et al 2000) for inorganic polymers.

7. REFERENCES

Alcorn A. 2003. *Embodied Energy and Carbon Dioxide Coefficients for New Zealand Building Materials*. Centre for Building Performance Research, Victoria University of Wellington, New Zealand.

Attiogbe EK, See HT and Miltenberger MA. 2001. 'Tensile Creep Characteristics in Restrained Shrinkage'. *Creep, Shrinkage and Durability Mechanics of Concrete and Other Quasi-Brittle Materials*. Proceedings of the Sixth International Conference, Elsevier Science, Amsterdam, Netherlands.

American Society for Testing and Materials. ASTM C 512 – 02 *Standard test method for creep of concrete in compression*. ASTM International, West Conshohocken, PA, USA.

American Society for Testing and Materials. C 1581 – 04 *Standard test method for determining age at cracking and induced tensile stress characteristics of mortar and concrete under restrained shrinkage*. ASTM International, West Conshohocken, PA, USA.

American Society for Testing and Materials. ASTM E 6 – 07 *Standard terminology relating to methods of mechanical testing*. ASTM International, West Conshohocken, PA, USA.

Barbosa VFF, MacKenzie KJD and Thaumaturgo C. 2000. 'Synthesis and Characterisation of Materials Based on Inorganic Polymers of Alumina and Silica: Sodium Polysialate Polymers'. *International Journal of Inorganic Materials* 2: 309–17.

Bissonnette B and Pigeon M. 1995. 'Tensile Creep at Early Ages of Ordinary, Silica Fume and Fiber Reinforced Concrete'. *Cement and Concrete Research* 25(5): 1075–85.

Davidovits J. 1991. 'Geopolymers: Inorganic Polymeric New Materials'. *Journal of Thermal Analysis* 37: 1633–56.

Gourley JT. 2003. *Geopolymers: Opportunities for Environmentally Friendly Construction Materials*. Institute of Materials Engineering Australasia 2003 Conference: Adaptive Materials for a Modern Society, Sydney, Australia (1–3 October 2003).

MacKenzie KJD. 2003. 'What Are These Things Called Geopolymers? A Physico-Chemical Perspective'. *Ceramic Transactions* 153: 175–86.

Mindess S and Young JF. 1981. *Concrete*. Prentice-Hall Inc, New Jersey, USA.

Neville AM. 1995. *Properties of Concrete* (4th edition). Addison Wesley Longman Limited, Harlow, UK.

Nicholson C, Fletcher R, Miller N, Stirling C, Morris J, Hodges S, MacKenzie K and Schumaker M. 2005. 'Building Innovation through Geopolymer Technology'. *Chemistry in New Zealand* (September): 10–12.

Gary Ong KC and Myint-Lay K. 2006. 'Application of Image Analysis to Monitor Very Early Age Shrinkage'. *ACI Materials Journal* 103(3): 169–176.

Ross AD. 1954. 'Experiments on the Creep of Concrete Under Two-Dimensional Stressing'. *Magazine of Concrete Research* (June): 3–10.

Ross AD. 1958. 'Creep of Concrete Under Variable Stress'. *Journal American Concrete Institute* 54: 739–58.

Standards Australia. AS 1012.13 – 1992 *Methods of test for concrete. Method 13: determination of the drying shrinkage of concrete for samples prepared in the field or laboratory*. SA, Sydney, Australia.

Standards Australia. AS 1012.16 – 1996 *Methods of testing concrete. Method 16:- Determination of creep of concrete cylinders in compression*. SA, Sydney, Australia.

Standards New Zealand. NZS 3112: Part 2:1986 *Methods of test for concrete – Tests relating to the determination of strength of concrete*. SNZ, Wellington, New Zealand.

Weiss J. 2006. 'Elastic Properties, Creep, and Relaxation'. In *Significance of Tests and Properties of Concrete and Concrete-Making Materials: STP 169D*. ASTM International, West Conshohocken, PA, USA.